ELSEVIER

Journal of Organometallic Chemistry 643–644 (2002) 89–97

Journal of Organometallic Chemistry

www.elsevier.com/locate/jorganchem

Fine tuning of the photophysical properties of cofacial diporphyrins via the use of different spacers

Frédéric Bolze [a,b], Claude P. Gros [b], Marc Drouin [a], Enrique Espinosa [b], Pierre D. Harvey [a,*], Roger Guilard [b,*]

[a] *Département de Chimie, Université de Sherbrooke, Sherbrooke, Quebec, Canada J1K 2R1*

[b] *LIMSAG (Laboratoire d'Ingénierie Moléculaire pour la Séparation et les Applications des Gaz, UMR 5633), Université de Bourgogne, Faculté des Sciences Gabriel, 6, Boulevard Gabriel, 21100 Dijon, France*

Received 8 June 2001; accepted 3 October 2001

Dedicated to Professor François Mathey

Abstract

The crystal and molecular structures of two unmetallated diporphyrin species using the biphenylene and dibenzofuran spacers, H_4(DPB) and H_4(DPO), respectively (DPB^{4-} = 1,8-bis[5-(2,8,13,17-tetraethyl-3,7,12,18-tetramethylporphyrinyl)]biphenylene; DPO^{4-} = 4,6-bis[5-(2,8,13,17-tetraethyl-3,7,12,18-tetramethylporphyrinyl)]dibenzofuran), are reported. These data are compared to their literature metallated analogs, stressing on the properties related to the flexibility of the ligands, π···π and M···M interactions. In addition, the lowest energy fluorescence properties of these non-phosphorescent diporphyrin compounds as well as three other related species, H_4(DPA), H_4(DPX), and H_4(DPS) (DPA^{4-} = 1,8-bis[5-(2,8,13,17-tetraethyl-3,7,12,18-tetramethylporphyrinyl)]anthracene; DPX^{4-} = 4,5-bis[5-(2,8,13,17-tetraethyl-3,7,12,18-tetramethylporphyrinyl)]-9,9-dimethylxanthene; DPS^{4-} = 4,6-bis[5-(2,8,13,17-tetraethyl-3,7,12,18-tetramethylporphyrinyl)]dibenzothiophene), have been examined both at room temperature in 2-MeTHF in the presence of Ar, air and O_2, and at 77 K. In all cases, the fluorescence arises from the $^1Q(\pi\pi^*)$, and the photophysical data at 77 and 298 K under Ar atmosphere correlate readily with the molecular geometry of these pincer ligands, where the non-radiative rate constants increase as the interplanar distances decrease. In the presence of dioxygen in solution, both the fluorescence lifetimes and quantum yields decrease as expected for quenching, with the second-order rate constants for bimolecular deactivation (k_Q) ranging from 0.9×10^{10} to 1.7×10^{10} s^{-1} M^{-1}. The H_4(DPB) compound exhibits the lowest k_Q indicating lesser ability for O_2 to interact with the interior of the diporphyrin cavity.

Keywords: Pacman porphyrins; Luminescence; Fluorescence; Oxygen quenching; RX structures

1. Introduction

Over the past two decades or so, the preparation and investigation of cofacial homobimetallic diporphyrins have been the subject of great interest [1–10], particularly for species with applications in the field of dioxygen [10–19] and dinitrogen [6] reduction, and activation of dihydrogen [4]. Different research groups employed various structural strategies to improve the performance of these reactions, e.g. by using heterobimetallic systems [1,5,20–22], or different spacers [23–25]. In the heterobimetallic series, the use of Al and Ga centers are used for their Lewis acid ability [20–22], and have shown some useful applications towards these directions. More recently, the use of different spacers has been made, and the role of the spacers, and more particularly their flexibility and size opening on the electrocatalytical and reactivity properties, was clearly demonstrated [24]. Taking advantage of the rich luminescence properties of the porphyrin unit [26] and its metallated analogs [27–32], our group demonstrated that the cofacial diporphyrin species and some of its metallated complexes are strongly luminescent [33], and even in one case, (DPA)Pd_2, can be used as an efficient

* Corresponding authors. Tel.: +1-81-9821-7092; fax: +1-81-9821-8017 (P.D.H.).

E-mail address: pharvey@courrier.usherb.ca (P.D. Harvey).

0022-328X/02/$ - see front matter
PII: S0022-328X(01)01346-8

O_2-sensor [34]. These literature findings clearly demonstrate that performance improvement for O_2 activation and O_2 sensorization strongly depends upon molecular tailoring.

We now wish to report the fluorescence properties of four cofacial diporphyrin compounds (H_4(DPB), H_4(DPO), H_4(DPS), and H_4(DPX)), and compare them with the recently reported H_4(DPA) (Chart 1) [33]. A clear correlation between the cavity size, relative flexibility and heavy atom effect, and the photophysical parameters will be shown. During the course of this work the crystal and molecular structure for H_4(DPB) and H_4(DPO) have been obtained from X-ray crystallography. The X-ray data, on one hand, were useful for the photophysical parameter analyses, and on the other hand, permitted an important comparison with other related metallated species. From these studies, evidence for weak π···π interactions will be provided for the DPB series, as well as M···M interactions for the literature data of metallated parent compounds.

2. Results and discussion

2.1. X-ray structure determination

The cofacial nature of H_4(DPB) and H_4(DPO) diporphyrin systems is well illustrated in Figs. 1 and 2 (see Table 1 for crystallographic data).

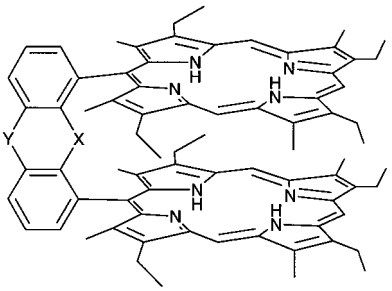

X = O, Y = CMe_2 : **H_4(DPX)**
X = O, Y = - : **H_4(DPO)**
X = S, Y = - : **H_4(DPS)**
X = -, Y = - : **H_4(DPB)**

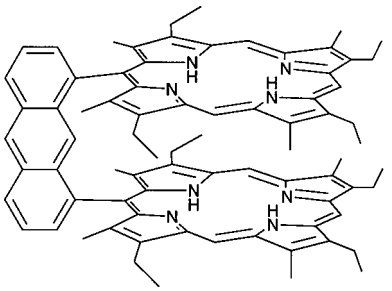

H_4(DPA)

Chart 1.

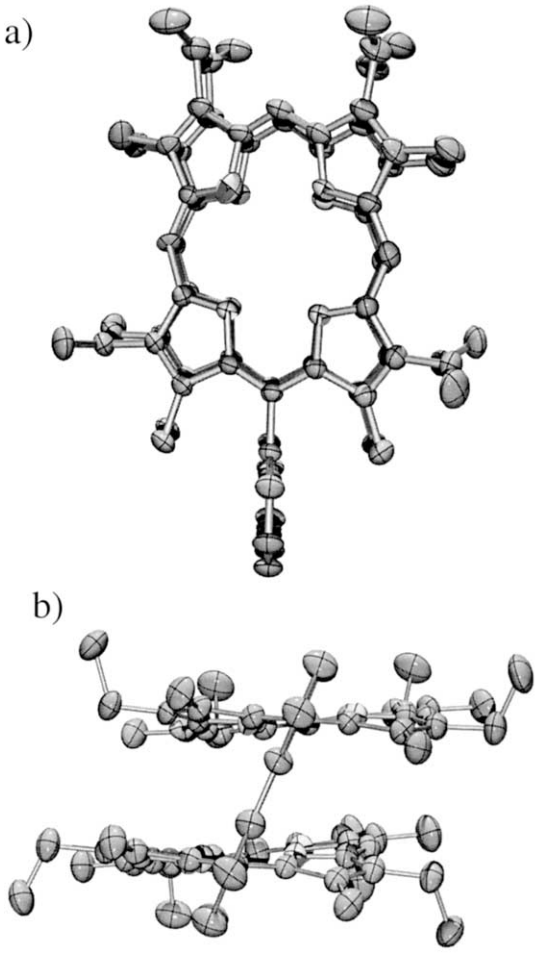

Fig. 1. ORTEP drawings for H_4(DPB). The ellipsoids are shown at 30% probability level. The H-atoms are not shown for clarity. Spheres represent atoms treated isotropically due to disorder. (a) Top view; (b) side view.

The macrocycles exhibit not only the typical sad/ruff [35] distortions, but the X-ray analyses also indicate that the rings are disordered over two sites for both porphyrins in H_4(DPO), and one cycle in H_4(DPB). The deviations of the C and N atoms away from the various porphyrin mean planes (PMP) are listed in Table 2, and range from 0.084 to 0.208 Å.

These data compare with those reported for the related H_4(DPA) molecule [36]. The role of the spacer on the structural parameters is clearly illustrated in Table 3.

The a–b, c–d, and Ct···Ct distances, and the interplanar angles (see definitions in Fig. 3) are 3.789, 3.804 and 3.958 Å and 3.9° for H_4(DPB), and 4.824, 5.528 and 6.904 Å, and 16.5°, for H_4(DPO), respectively.

These data are consistent with the 'quasi-parallel' and 'open mouth' geometries of the DPB and DPO spacers. The decrease in slip angle (26.2–8.3°) and lateral shift (1.75–1.00 Å) going from H_4(DPB) to H_4(DPO) implies that stabilizing π···π contacts must

occur in the former, but not in the latter. The parallel geometry of the rings in H_4(DPB) favors these interactions, which is not the case for the 'open mouth' structure offered by the H_4(DPO) system. The structure of H_4(DPA) analyzed recently also reports a larger slip angle (22.9°) and lateral shift (2.33 Å), which support the evidence for π···π interactions. Although one may argue that coincidental crystal packing forces are the cause for these apparent interactions in the crystals, the spectroscopic findings for solutions presented below, also support this π···π model.

These X-ray studies offer a unique opportunity to address the role of metallation on the structural parameters, for two very different spacers. In the H_4(DPB) series, two metallated complexes are known

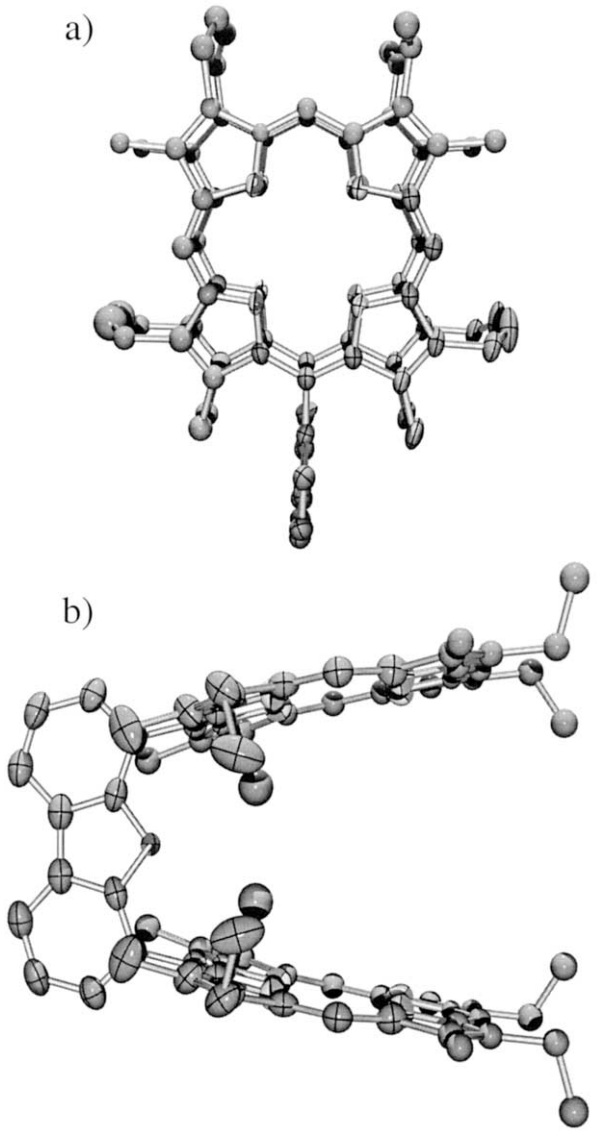

Fig. 2. ORTEP drawings for H_4(DPO). The ellipsoids are shown at 30% probability level. The H-atoms are not shown for clarity. Spheres represent atoms treated isotropically due to disorder. (a) Top view; (b) side view.

Table 1
Crystal data and structure refinement parameters for H_4(DPB) and H_4(DPO)

	H_4(DPB)	H_4(DPO)
Empirical formula	$C_{70}H_{80}N_8$	$C_{76}H_{80}N_8O{\cdot}2C_7H_{14}$
Formula weight	1155.08	1321.88
Temperature (K)	293(1)	110(2)
Wavelength (Å)	1.54184	0.71070
Radiation	Cu–K_α	Mo–K_α
Space group	$P\bar{1}$	$P2_1/m$
Unit cell dimemsions		
a (Å)	12.102(5)	13.2795(3)
b (Å)	13.380(7)	20.7046(5)
c (Å)	21.418(19)	14.7135(3)
α (°)	76.76(4)	90
β (°)	81.90(6)	109.885(1)°
γ (°)	65.09(4)	90°
V (Å^3)	3058(3)	3804.2(2)
Z	2	2
ρ_{calc} (g cm^{-3})	1.146	1.154
Absorption coefficient (mm^{-1})	0.539	0.068
Crystal size (mm)	$0.25\times0.15\times0.10$	$0.25\times0.20\times0.10$
Final $R(F)$ indices $[I_{(net)}\geq2.0\sigma(I_{net})]$ [a]	0.0946	0.1066
Final $R_w(F^2)$ indices $[I_{(net)}\geq2.0\sigma(I_{net})]$ [b]	0.2755	0.2556

.2755 > 0.2556

[a] $R(F)=(\Sigma_i\,||F_{obs}|_i-|F_{calc}|_i|)/(\Sigma_i|F_{obs}|_i|)$.

[b] $R_w(F^2)=\sqrt{[(\Sigma_i\{w_i(F^2_{i,\,obs}-F^2_{i,\,calc})\}^2)/(\Sigma_i\{w_i(F^2_{i,\,obs})\}^2)]}$.

Table 2
Comparison of the PMP for various cofacial diporphyrins [a]

Compound	Molecule	PMP		Reference
		First ring	Second ring	
H_4(DPB)	–	0.1690 [b]	0.1952	t.w.
		0.2076 [b]		
H_4(DPO)	–	0.0841	0.0841 [c]	t.w.
		0.1575	0.1575 [c]	
H_4(DPA)	#1	0.1857	0.1285	[36]
H_4(DPA)	#2	0.2312	0.2524	[36]

t.w. = this work.

[a] In Å.

[b] The first ring is disordered over two sites.

[c] Both rings are related by a symmetry plane in the unit cell. Data for two rings are provided as disorder is found possible for the C atoms.

(M = Co [37], Cu [8]). The most striking feature in Table 3 is the change in d(Ct···Ct) where this datum is greater for the unmetallated H_4(DPB) molecule. In addition, the smaller d(M···M) values with respect to d(Ct···Ct) strongly suggest that weak M···M attractions must occur, complementing the potential M···π interactions [38]. The presence of these interactions is also felt in the changes for the other structural parameters (slip angle, lateral shift, a–b and c–d distances). The *exo*-coordinations of Cl and OEt on Mn and Al in

Table 3
Selected structural data for H_4(DPB) and H_4(DPO) and their metallated derivatives

Compound	d(Ct···Ct) (Å)	d(M···M) (Å)	Interplanar angle (°)	Slip angle (°)	Lateral shift (Å)	a–b distance (Å)	c–d distance (Å)	Reference
H_4(DPB) [a]	3.958	–	3.9	26.2	1.75	3.789	3.804	t.w.
(DPB)Cu_2	3.862	3.807	4.4	25.0	1.63	3.797	3.802	[8]
(DPB)Co_2	3.769	3.727	4.3	23.8	1.52	3.785	3.778	[37]
(DPB)(CuMn)·Cl	3.916	4.126	5.2	25.7	1.70	3.770	3.814	[21]
(DPB)(CoAl)·OEt	4.083	4.370	7.4	29.8	2.03	3.778	3.821	[20]
(DPB)$(Lu(OH))_2$·CH_3OH	5.542	3.526	27.1	13.9	1.33	3.849	4.176	[40]
H_4(DPO) [b]	6.904	–	16.5	8.3	1.00	4.824	5.528	t.w.
(DPO)Zn_2·CH_3OH·CH_2Cl_2	7.587	7.775	29.6	20.6	2.67	5.003	5.536	[25]
(DPO)(Fe_2-μ-O_2)	4.611	3.504	(22.9) [c]	(10.4) [d] (−11.0) [d]	–[d]	4.764	5.082	[25]
(DPO)Co_2·2MeOH·CH_2Cl_2	8.874	8.624	56.5	18.5 5.1	2.54	4.825	5.731	[24]

[a] The N atoms are located on six sites due to disorder. All calculations were performed considering these sites. Two sites for the rings were averaged.
[b] The porphyrin rings are disordered, and the reported data are average values for all possible sites.
[c] The macrocycle planes are twisted side way, so this angle is not defined by the spacer as shown in Fig. 3.
[d] Because of the side way twisted planes, two different angles are obtained, and no lateral shift exists.

(DPB)(CuMn)·Cl and (DPB)(CoAl)·OEt, respectively, have the effect of moving the penta-coordinated metal atom away from the PMP. Consequently, the M···M′ separations are increased, and interactions weakened. The longer d(Ct···Ct), and d(M···M) and c–d data (Table 3) witness the weakness in M···M′ attractions (and M···π as well). The (DPB)$(Lu(OH))_2$·MeOH system is different as the *endo*-coordination of hydroxyl and methanol groups on the Lu metals occur. This particular example clearly illustrates the impressive flexibility of the H_4(DPB) free base, promoting inter-ring interactions (π···π, M···M, M···π), and strong bridging coordinations of small ligands inside the cavity.

For the DPO series, the only metallated version known to us is (DPO)Zn_2·MeOH·CH_2Cl_2 [25]. In this case, the M···M and Ct···Ct distances are exceedingly large (about 7.7 and 7.6 Å, respectively), and no inter-ring interaction is anticipated. For the free base, the Ct···Ct value is shortened to 6.9 Å. Owing to the presence of a MeOH molecule inside the cavity of the former, the effect of metallation cannot be addressed with these structures. In the 'coordinated' series, two *endo*-metallated diporphyrin DPO systems have been reported recently by Nocera and coworkers [11–23]. These two examples strongly differ from the nature of the ligands. In the first case, (DPO)(Fe_2-μ-O), an μ-oxo bridging anion is located inside the cavity, and distort the 'open mouth' geometry strongly, with short d(Ct···Ct) and d(M···M) of 4.622 and 3.504 Å, respectively. Conversely, (DPO)Co_2·2MeOH exhibits methanol molecules inside the cavity, and the d(Ct···Ct) and d(M···M) distances increase up to record high values of values 8.874 and 8.624 Å, respectively. These data further illustrate the great flexibility of these free bases, and must be taken into account when analyzing the physical and chemical properties such as those described in Section 1.

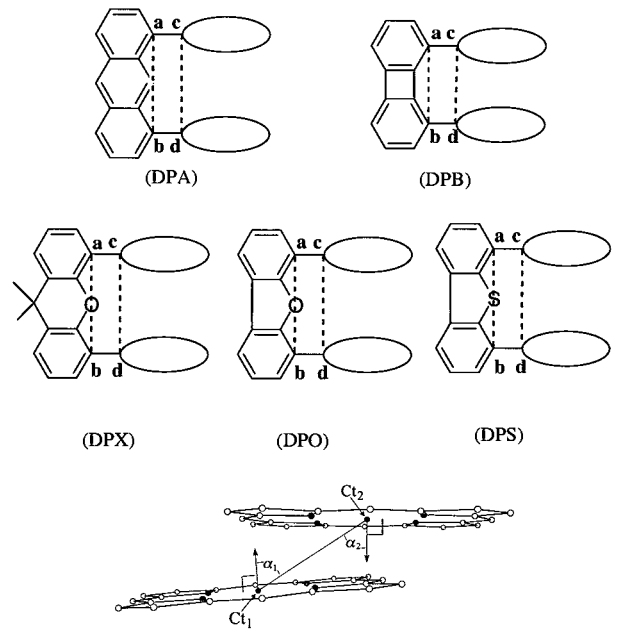

Fig. 3. Top: the series of aromatic linking units used to join porphyrin monomers to form the cofacial porphyrin dimers, where the a–b and c–d distances are defined. Bottom: illustration of the method by which the selected crystallographically derived geometrical features were measured. Macrocyclic centers (C_t) were calculated as the centers of the 4N planes for each macrocycle. The interplanar angles were measured as the angle between the two macrocyclic 24-atom least-squares planes. The slip angles (α) were calculated as the average angle between the vector joining the two rings and the unit vectors normal to the two macrocyclic 24 atoms least-squares planes ($\alpha = (\alpha_1 + \alpha_2)/2$). Lateral shift was defined as [$\sin(\alpha) \times (C_t - C_t$ distance)].

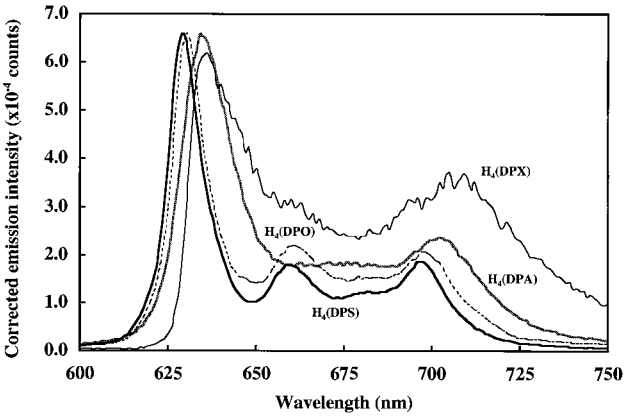

Fig. 4. Fluorescence spectra of H_4(DPA) (gray), H_4(DPS) (bold), H_4(DPO) (dashed), H_4(DPX) (normal) in 2-MeTHF at 298 K under Ar atmosphere.

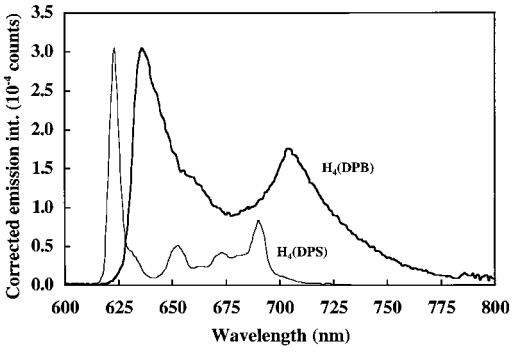

Fig. 5. Fluorescence spectra of H_4(DPB) (bold) and H_4(DPS) (normal) in 2-MeTHF at 77 K.

2.2. Fluorescence study

The emission spectra of selected diporphyrins at 298 and 77 K are shown in Figs. 4 and 5, respectively, and exhibit the typical vibronic structure associated with the porphyrinic fragment. These bands are the mirror image of the absorption bands (data in Table 4), and the excitation spectra superimpose these absorptions as well. In addition, the Stokes shifts (Table 5) are very small, and the emission lifetimes (described below) are all in the ns regime. All these observations confirm that the observed luminescences are fluorescences arising from the lowest energy $^1Q(\pi\pi^*)$ states. Although the porphyrin environment is practically identical in all cases, the position of the 0–0 peaks is a function of the spacer. For example, the 77 K 0–0 fluorescence data for H_4(DPA) and H_4(DPB) are 624 and 636 nm, respectively. Both spacers are rigid and the crystal structure reveals that the interplanar angles are about 2° for H_4(DPA) [36] and 4° for H_4(DPB) (this work, see Table 3). The macrocycles are therefore approximately parallel to each other, and π···π contacts occur over a large surface of the porphyrin planes, as well illustrated in Fig. 1 for H_4(DPB). Using a simplified MO model (Fig. 6), π···π interactions between the two planar π systems lead to the formation of new π and π* MOs.

The HOMO–LUMO energy gap is smaller in the dimer, in comparison with a non- or weakly interacting porphyrin. The lowest energy electronic transition (π → π*) is anticipated to be red shifted in interacting systems. For the 'open mouth' diporphyrins (H_4(DPO) and H_4(DPS)), such π···π contacts are different as an important deviation from coplanarity is reported for (DPO)M_2 systems (see Table 3 for details). Therefore, comparison is difficult. Nonetheless the 0–0 positions of the H_4(DPA), H_4(DPS), and H_4(DPO) compounds are the largest, which is consistent with this model. For the more flexible xanthene spacer derivative H_4(DPX), the X-ray data reported for the metallated (DPX)Co_2 species indicate that the a–b and c–d distances (4.634 and 4.404 Å, respectively) [23,24] are shorter than those of (DPA)Co_2 (4.949 and 4.920 Å, respectively) [36] and (DPO)Zn_2 (5.003 and 5.576 Å, respectively) [25], but larger than those of (DPB)Co_2 (3.185 and 3.778 Å [37], respectively). The intermediate values for the position of the 0–0 peak in H_4(DPX) also appear to be directed by the π···π contact arguments.

For convenience, the following description of photophysical properties will be presented taking into account the a–b and c–d parameters. The H_4(DPB), the H_4(DPX) and the H_4(DPA), and the H_4(DPO) and H_4(DPS) species exhibit small, medium and large a–b

Table 4
UV–vis data for the diporphyrins [a]

Compound	Soret region	λ_{max} (nm) (ε, $\times 10^{-3}$ M^{-1} cm^{-1})			
		Q bands			
H_4(DPB) [b]	379 (173.9)	511 (6.3)	540 (2.0)	580 (3.4)	632 (1.8)
H_4(DPX)	380 (200)	508 (12.0)	543 (5.4)	578 (6.0)	628 (2.3)
H_4(DPA) [b]	395 (190.5)	506 (14.1)	539 (5.1)	578 (6.0)	631 (3.3)
H_4(DPS)	400 (316)	502 (28.1)	536 (13.7)	571 (12.2)	623 (5.6)
H_4(DPO)	396 (260)	502 (24)	536 (12.0)	572 (1.1)	624 (5.0)

[a] CH_2Cl_2, 298 K.
[b] Benzene, 298 K.

Table 5
Selected electronic spectroscopic data [a]

Compounds	0–0 Absorption (nm)		0–0 Fluorescence (nm)		Stoke shifts (cm^{-1})	
	298 K	77 K	298 K	77 K	298 K	77 K
H_4(DPB)	631	631	641	636	250	130
H_4(DPX)	631	630	636	634	130	100
H_4(DPA) [b]	629	621	634	624	130	80
H_4(DPO)	627	622	629	623	50	30
H_4(DPS)	626	620	629	623	80	80

[a] In 2-MeTHF at 77 K. The uncertainties on λ is ± 1 nm.
[b] Data extracted from Ref. [33].

and c–d distances, respectively. The photophysical properties of the cofacial diporphyrins are shown in Table 6 for the 298 K/Ar data and Table 7 for the 77 K ones.

The fluorescence lifetimes (τ_F) and quantum yields (Φ_F) at 298 K (Table 6) vary as H_4(DPB) < H_4(DPX) < H_4(DPA) < H_4(DPS) < H_4(DPO), following the same trend as the a–b and c–d parameters. These results demonstrate that the ring···ring interactions are clearly present, affecting the excited state deactivation processes. The greater the π···π interactions, the greater the intramolecular excited state deactivations are. The radiative (k_F) and non-radiative (k_{nr}) also follow this trend, as expected. The fine tuning in τ_F and Φ_F, H_4(DPX) < H_4(DPA), and H_4(DPS) < H_4(DPO) reflects a greater flexibility in H_4(DPX) (compared with H_4(DPA)) and the heavy atom effect on the S_1 state (S vs. O) [39]. At 77 K (Table 7), a similar trend is observed (leading to the same conclusion), with the exception that τ_F for H_4(DPO) is unexpectedly lower (the data were reproduced four times). While a sensitive decrease is observed for k_{nr} going from 298 to 77 K, consistent with the gain in medium rigidity, the k_F data are predictably more or less constant considering the uncertainties.

The ability to interact with O_2, using typical bimolecular O_2 quenching experiments, was also investigated. The second-order rate constants to molecular deactivation, k_Q, were extracted from Stern–Volmer plots using solution bubbled with Ar, air and dioxygen (Table 8).

The plots exhibited correlation coefficients of 0.99 or even better, and both τ_F and Φ_F were found to decrease with the concentration of O_2, as anticipated. Owing to lower uncertainties, (6% using τ_F data vs. 20% using Φ_F), only the k_Q based on τ_F are reported. The magnitude of these rate constants (10^{10} s^{-1} M^{-1}) is indicative of efficient quenching occurring at the diffusion limit.

The data can be divided into two series: (1) H_4(DPB), lower k_Q; and (2) H_4(DPX), H_4(DPA), H_4(DPO) and H_4(DPS), similar to each other considering the uncertainties, but higher k_Q. The interpretation of these results introduces the idea that *endo*- and *exo*-O_2···porphyrin interactions occur. With a significantly smaller cavity opening (the a–b, c–d, and Ct···Ct distances are 3.789, 3.804, and 3.958 Å, respectively), the penetration of O_2 inside the sandwich structure H_4(DPB) is much less favored (but not precluded). On the other hand, the four other diporphyrin species, which exhibit relatively similar k_Q data, seem to provide sufficient space (or flexibility) to allow O_2 to penetrate the cavity. This observation is consistent with the numerous X-ray data of metallated diporphyrins species that exhibit ions or neutral molecules inside the pincer, using spacers such as DPA^{4-} and DPO^{4-}.

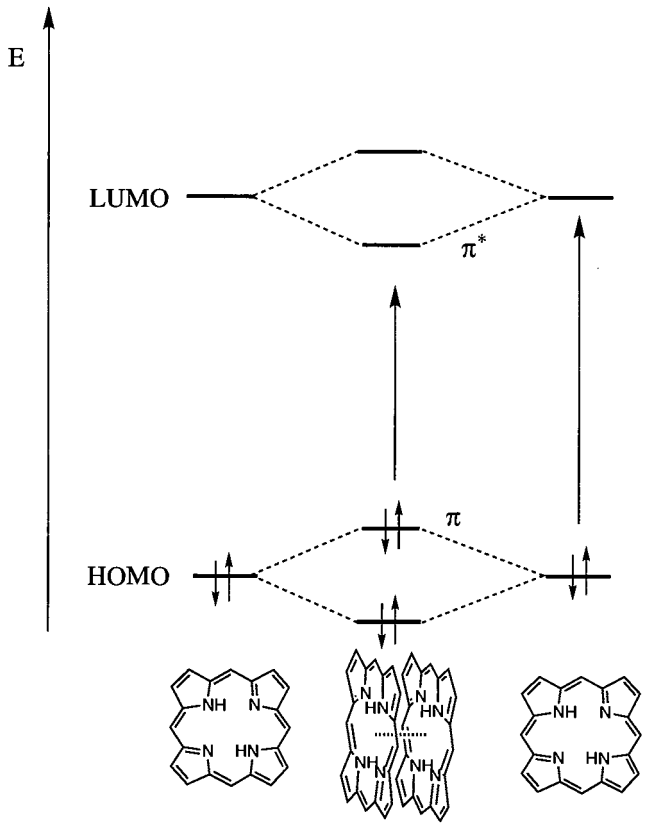

Fig. 6. Simplified MO model illustrating the effect of the two interacting porphyrins via π···π staking on the HOMO–LUMO.

Table 6
Photophysical parameters for the cofacial diporphyrins in fluid solutions [a]

Compounds	τ_F (ns)	Φ_F	k_F (s^{-1})	k_{nr} (s^{-1})
H_4(DPB)	10.0	0.0040	0.40×10^6	10.0×10^7
H_4(DPX)	12.4	0.011	0.80×10^6	8.0×10^7
H_4(DPA) [b]	14.1	0.020	1.4×10^6	6.9×10^7
H_4(DPS)	16.9	0.035	2.2×10^6	5.7×10^7
H_4(DPO)	17.7	0.045	2.5×10^6	5.4×10^7

[a] In 2-MeTHF at 298 K under Ar atmosphere. The uncertainties are ±0.3 ns for τ_F and $\pm10\%$ for Φ_F.
[b] Data extracted from Ref. [33].

Table 7
Photophysical parameters for the cofacial diporphyrins in low temperature matrix [a]

Compounds	τ_F (ns)	Φ_F	k_F (s^{-1})	k_{nr} (s^{-1})
H_4(DPB)	17.0	0.012	0.70×10^6	5.9×10^7
H_4(DPX)	17.0	0.026	1.5×10^6	5.7×10^7
H_4(DPA) [b]	24.0	0.044	1.8×10^6	3.9×10^7
H_4(DPS)	23.6	0.055	2.3×10^6	3.4×10^7
H_4(DPO)	20.7	0.058	2.8×10^6	4.5×10^7

[a] In 2-MeTHF at 77 K. The uncertainties are ±0.3 ns for τ_F and $\pm10\%$ for Φ_F.
[b] Data extracted from Ref. [33].

Table 8
Effect of dioxygen on the photophysical parameters [a]

Compound	k_Q ($s^{-1}\,M^{-1}$) (based on τ_F)
H_4(DPB)	0.9×10^{10}
H_4(DPX)	1.4×10^{10}
H_4(DPA)	1.7×10^{10}
H_4(DPS)	1.6×10^{10}
H_4(DPO)	1.4×10^{10}

[a] In 2-MeTHF at 298 K. The uncertainties are ±0.3 ns on τ_F, which lead to uncertainties of $\pm6\%$ on k_Q (or 0.1×10^{10}).

For the DPB^{4-} series, this occurs rarely and only one exception to the trend is found in $(DPB)(Lu(OH))_2$ [40].

3. Experimental

3.1. Materials

H_4(DPA), H_4(DPB), H_4(DPO), and H_4(DPX) were synthesized according to the literature methods [1–23,41]. The solvents were 'reagent grade' and were used without further purification. The 2-MeTHF and EtOH used for the spectroscopic and photophysical studies were distilled over sodium under nitrogen prior to use.

3.1.1. Synthesis of H_4(DPS)

To a solution of 1,8-bis[(4,4′-diethyl-3,3′-dimethyl-2,2′-dipyrryl)methyl]dibenzothiophene [42] (2.70 g, 4.2 mmol) and 5,5′-diformyl-3,3′-diethyl-4,4′-dimethyl-2,2′-dipyrrylmethane (2.50 g, 8.8 mmol) in MeOH (800 ml), 250 ml of a solution of *para*-toluene sulfonic acid (10 g, 52 mmol) in MeOH was added during 18 h. The dark red solution was stirred under Ar for 12 h. *O*-Chloranil (3 g) was added, and the solution was stirred in air for 1 h. The mixture was dried and redissolved in 200 ml of CH_2Cl_2. A saturated methanolic solution of $Zn(OAc)_2{\cdot}2H_2O$ (10 ml) was added and the mixture was refluxed for 15 min. The zinc derivative was isolated by column chromatography on silica gel (CH_2Cl_2). Demetallation by 6 M HCl afforded the free base bisporphyrin which was further purified by chromatography (silica gel, CH_2Cl_2–MeOH 100:0 to 50:50 in volume). Purple microcrystals of pure bisporphyrin were obtained in 18.0% yield ($m = 850$ mg). Anal. Found: C, 79.94; H, 6.77; N, 9.41; S, 2.91. Calc. for $C_{76}H_{80}N_8S$: C, 80.24; H, 7.09; N, 9.85; S, 2.82%. ^{1}H-NMR ($CDCl_3$, δ ppm): 9.84 (s, 4H), 9.65 (s, 2H), 8.82 (d, 2H), 7.95 (m, 4H), 3.85 (q, 16H), 3.40 (s, 12H), 2.37 (s, 12H), 1.64 (t, 12H), 1.62 (t, 12H), −3.65 (large, s, 2H), −3.78 (large, s, 2H). MS (MALDI-TOF); m/z: 1138 $[M]^+$. UV–vis: λ_{max} (nm) (ε, 10^{-3} $M^{-1}\,cm^{-1}$) (CH_2Cl_2): 400 (316), 502 (28.0), 536 (14.0), 571 (12.0), 623 (5.6).

3.2. Instrumentation and methods

The 298 K spectra were recorded in a Varian Cary 1 spectrophotometer using a standard 1 cm^2 quartz cell. The luminescence spectra (excitation and emission) were acquired in a double monochromator Fluorolog 1902 instrument from Spex. The source was a 400 W Hg–Xe high-pressure lamp. All spectra were automatically corrected by the instrument software for the spectrophotometer response. Fluorescence lifetimes were measured using a single photon counting apparatus from PTI equipped with an N_2 flash lamp pulsing at 10 kHz. The pulse width was of the order of 2.5 ns and τ_F were obtained using deconvolution techniques. Quantum yields were measured using ruthenium(II) tris(-bipyridine)chloride as the standard ($\Phi = 0.376 \pm 0.036$) [43–46]. The samples were dissolved in 2-MeTHF and the standard in EtOH for solubility reasons. As the two solvents were different, the following correction formula for Φ was used [47]:

$$\Phi_{em}^{spl} = \Phi_{em}^{std}\left(\frac{A^{std}}{A^{spl}}\right)\left(\frac{I^{spl}}{I^{std}}\right)\left(\frac{n_D^{spl}}{n_D^{std}}\right)^2$$

The procedure involves the use of solutions with identical or nearly identical known optical densities, for both the samples and standards, in the 0.04 absorption range.

3.3. Crystallography

H_4(DPB) and H_4(DPO) were recrystallized by slow evaporation of a concentrated solution in CH_2Cl_2–heptane. Intensity data from the dark prism crystals were collected at 293(1) K in an Enraf–Norrius CAD-4 automatic diffractometer for H_4(DPB), and at 110(2) K in an Enraf–Norrius KappaCCD for H_4(DPO). Table 1 provides the crystallographic and data collection details. Cell constants and an orientation matrix for data collection were obtained from a least-squares refinement using the setting angles of 24 centered reflections in the range $40° \leq 2\theta \leq 50°$ (H_4(DPB)) and of all collected reflections in the range $2\theta \leq 42°$ (H_4(DPO)). In both structures, space group determination was based upon systematic absences, packing considerations, a statistical analysis of intensity distribution, and the successful solution and refinement of the structure. The NRCCAD and COLLECT programs [48] were used for centering, indexing, and data collections of H_4(DPB) and H_4(DPO), respectively. Two standard reflections were measured every 60 min throughout data collection in H_4(DPB). The NRCVAX [49] and SHELXS-97 [50] programs were respectively used for the crystal structure solution of H_4(DPB) and H_4(DPO) by the application of direct methods. The SHELXL-97 program [50] was used for the refinement of both structures by full-matrix least-squares on F^2. No significant decay was observed during data collections. Isotropic extinction coefficients were included in the refinements to account for secondary extinction effects [51]. In both structures, hydrogen atoms were all geometrically placed and the respective final refinements included anisotropic thermal parameters for the non-hydrogen atoms (except for those involved in disorder), and isotropic thermal parameters for the hydrogen atoms. Individual displacement parameters were fixed at $U_H = 1.5 \times U_{eq}$ (C-methyl, OH) and at $U_H = 1.2 \times U_{eq}$ (C and N) for refinements. The $R(F)$ and $R_w(F^2)$ final discrepancy indices at convergence for the $I_{net} \geq 2.0\sigma(I_{net})$ significant reflections, the number of restraints and variables, and the goodness-of-fit (GoF) are listed in Table 1.

3.3.1. Crystal data for H_4(DPO)

$C_{90}H_{112}N_8O$, $M = 1321.88$, monoclinic, $a = 13.2795(3)$ Å, $b = 20.7046(5)$ Å, $c = 14.7135(3)$ Å, $\beta = 109.885(1)°$, $U = 3804.2(2)$ Å^3, $T = 110(2)$ K, space group $P2_1/m$, $Z = 2$, $\mu = 0.068$ mm^{-1}, 15 338 measured reflections, 4051 independent ($R_{int} = 0.087$), 3241 with $I_{net} > 2\sigma I_{net}$. The final $R(F)$ and $R_w(F^2)$ agreement factors were 0.107 and 0.256, respectively. The crystal structure is disordered. It was refined using several restraints (option SAME in SHELXL-97) to avoid unrealistic geometries. Both macrocycles were found to be disordered where the C and N atoms occupy the two sites.

3.3.2. Crystal data for H_4(DPB)

$C_{76}H_{30}N_8$, $M = 1055.08$, triclinic, $a = 12.102(5)$ Å, $b = 13.380(7)$ Å, $c = 21.418(19)$ Å, $\alpha = 76.76(4)°$, $\beta = 81.90(6)°$, $\gamma = 65.09(4)°$, $U = 3058(3)$ Å^3, $T = 293$ K, space group $P\bar{1}$, $Z = 2$, $\mu = 0.539$ mm^{-1}, 9883 measured reflections, 9384 independent ($R_{int} = 0.074$), 5674 with $I_{net} > 2\sigma I_{net}$. The final $R(F)$ and $R_w(F^2)$ agreement factors were 0.095 and 0.275, respectively. The crystal structure is disordered. It was refined using several restraints (option SAME in SHELXL-97) to avoid unrealistic geometries. One of the macrocycle was found to be disordered where the C and N atoms occupy the two sites.

4. Conclusion

This work provides evidence that the two porphyrin macrocycles in the cofacial systems can interact via π···π contacts, and that these interactions can be varied via the use of an appropriate spacer. These interactions can be monitored using spectroscopic and photophysical methods as well as by crystallography. Such structural and photophysical investigations proved important for the design of 'more performing' molecular devices for O_2 reduction and O_2 sensitization, where M···M distances, and the facility for substrates to penetrate the cavity, can be tailored. The comparison of the X-ray data of the free base with the metallated DPB series provided clear and unprecedented evidence for weak M···M and M···π interactions in these cofacial diporphyrin systems. The role of these interactions shall prove to be important in the chemical processes.

5. Supplementary material

Crystallographic data for structural analysis have been deposited with the Cambridge Crystallographic Data Centre, CCDC nos. 164712 and 164713 for H_4(DPB) and H_4(DPO), respectively. Copies of this information may be obtained free of charge from The Director, CCDC, 12 Union Road, Cambridge, CB2 1EZ, UK (Fax: +44-1223-336033; e-mail: deposit@ccdc.cam.ac.uk or www: http://www.ccdc.cam.ac.uk).

Acknowledgements

P.D.H. thanks NSERC (Natural Sciences and Engineering Research Council of Canada) and the 'Ministère des Relations Internationales du Québec' for financial support. The support of the CNRS (R.G., UMR 5633) and the 'Ministère de l'Education Nationale, de la Recherche et de la Technologie' are also acknowledged. E.E. thanks CNRS (Centre National de la Recherche Scientifique) for financial support.

References

[1] S. Brandès, Thèse de l'Université de Bourgogne, Dijon, 1993.
[2] C.K. Chang, I. Abdalmuhdi, Angew. Chem. Int. Ed. Engl. 23 (1984) 164.
[3] J.P. Collman, K. Kim, C.R. Leidner, Inorg. Chem. 26 (1987) 1152.
[4] J.P. Collman, J.E. Hutchison, P.S. Wagenknecht, N.S. Lewis, M.A. Lopez, R. Guilard, J. Am. Chem. Soc. 112 (1990) 8206.
[5] J.P. Collman, J.M. Garner, J. Am. Chem. Soc. 112 (1990) 166.
[6] J.P. Collman, J.E. Hutchison, M.A. Lopez, R. Guilard, R.A. Reed, J. Am. Chem. Soc. 113 (1991) 2794.
[7] S.S. Eaton, G.R. Eaton, C.K. Chang, J. Am. Chem. Soc. 107 (1985) 3177.
[8] J.P. Fillers, K.G. Ravichandran, I. Abdalmuhdi, A. Tulinsky, C.K. Chang, J. Am. Chem. Soc. 108 (1986) 417.
[9] J.E. Hutchison, Thesis, Stanford, 1991.
[10] J.P. Collman, A.O. Chong, G.B. Jamieson, R.T. Oakley, E. Rose, E.R. Schmittou, J.A. Ibers, J. Am. Chem. Soc. 103 (1981) 516.
[11] C.K. Chang, Chem. Commun. (1977) 800.
[12] C.K. Chang, H.-Y. Liu, I. Abdalmuhdi, J. Am. Chem. Soc. 106 (1984) 2725.
[13] J.P. Collman, P. Denisevich, Y. Konai, M. Marrocco, C. Koval, F.C. Anson, J. Am. Chem. Soc. 102 (1980) 6027.
[14] R.R. Durand Jr., C.S. Bencosme, J.P. Collman, F.C. Anson, J. Am. Chem. Soc. 105 (1983) 2710.
[15] K. Kim, Thesis, Stanford, 1987.
[16] Y. Le Mest, M. L'Her, J.-Y. Saillard, Inorg. Chim. Acta 248 (1996) 181.
[17] Y. Le Mest, C. Inisan, A. Laouenan, M. L'Her, J. Talarmin, M. El Kalifa, J.-Y. Saillard, J. Am. Chem. Soc. 119 (1997) 6095.
[18] H.-Y. Liu, I. Abdalmuhdi, C.K. Chang, F.C. Anson, J. Phys. Chem. 89 (1985) 665.
[19] L.M. Proniewicz, J. Odo, J. Goral, C.K. Chang, K. Nakamoto, J. Am. Chem. Soc. 111 (1989) 2105.
[20] R. Guilard, M.A. Lopez, A. Tabard, P. Richard, C. Lecomte, S. Brandès, J.E. Hutchison, J.P. Collman, J. Am. Chem. Soc. 114 (1992) 9877.
[21] R. Guilard, S. Brandès, A. Tabard, N. Bouhmaida, C. Lecomte, P. Richard, J.M. Latour, J. Am. Chem. Soc. 116 (1994) 10202.
[22] R. Guilard, S. Brandès, C. Tardieux, A. Tabard, M. L'Her, C. Miry, P. Gouerec, Y. Knop, J.P. Collman, J. Am. Chem. Soc. 117 (1995) 11721.
[23] C.J. Chang, Y. Deng, A.F. Heyduc, C.K. Chang, D.G. Nocera, Inorg. Chem. 39 (2000) 959.
[24] C.J. Chang, Y. Deng, C. Shi, C.K. Chang, F.C. Anson, D.G. Nocera, Chem. Commun. (2000) 1355.
[25] Y. Deng, C.J. Chang, D.G. Nocera, J. Am. Chem. Soc. 122 (2000) 410.
[26] M. Gouterman, J. Mol. Spectrosc. 6 (1961) 138.
[27] J. Aaviksoo, A. Freiberg, S. Savikhin, G.F. Stelmakh, M.P. Tsvirko, Chem. Phys. Lett. 111 (1984) 275.
[28] A. Antipas, D. Dolphin, M. Gouterman, E.C. Johnson, J. Am. Chem. Soc. 100 (1978) 7705.
[29] E.M. Ebeid, A.M. Habib, M.H. Abdel-Kader, A.B. Yousef, R. Guilard, Spectrochim. Acta A 44 (1988) 127.
[30] M. Ikonen, D. Guez, V. Marvaud, D. Markovitsi, Chem. Phys. Lett. 231 (1994) 93.
[31] D. Kim, J. Terner, T.G. Spiro, J. Am. Chem. Soc. 108 (1986) 2097.
[32] O. Ohno, Y. Kaizu, H. Kobayashi, J. Chem. Phys. 82 (1985) 1779.
[33] P.D. Harvey, N. Proulx, G. Martin, M. Drouin, D.J. Nurco, K.M. Smith, F. Bolze, C.P. Gros, R. Guilard, Inorg. Chem. 40 (2001) 4134.
[34] F. Bolze, C.P. Gros, P.D. Harvey, R. Guilard, J. Porphyrins Phthalocyanines 5 (2001) 569.
[35] W. Jentzen, X.Z. Song, J.A. Shelnutt, J. Phys. Chem. B 101 (1997) 1684.
[36] F. Bolze, M. Drouin, P.D. Harvey, C.P. Gros, R. Guilard, submitted for publication.
[37] J.P. Collman, J.E. Hutchison, M.A. Lopez, A. Tabard, R. Guilard, W.K. Seok, J.A. Ibers, M. L'Her, J. Am. Chem. Soc. 114 (1992) 9869.
[38] In a recent review, M···M interactions above the sum of the van der Wals radii, are in fact common, where ν(M···M) vibrations have been securely localized by mean of Resonance Raman, or polarized light Raman measurements on single crystals. P.D. Harvey, Coord. Chem. Rev. 153 (1996) 175.
[39] N.J. Turro, Modern Molecular Photochemistry, Benjamin/Cummings, Menlo Park, CA, 1978.
[40] M. Lachkar, A. Tabard, S. Brandès, R. Guilard, A. Atmani, A. De Cian, J. Fischer, R. Weiss, Inorg. Chem. 36 (1997) 4141.
[41] M.A. Lopez, Thèse de l'Université de Bourgogne, Dijon, 1990.
[42] K.M. Kadish, C.P. Gros, F. Bolze, J.M. Barbe, F. Jerôme, Z. Ou, J. Shao, R. Guilard, in preparation.
[43] J.N. Demas, G.A. Crosby, J. Am. Chem. Soc. 93 (1971) 2841.
[44] P. Hartmann, W. Trettnak, Anal. Chem. 68 (1996) 2615.
[45] J.V. Houten, R.J. Watts, J. Am. Chem. Soc. 98 (1976) 4853.
[46] R.J. Watts, G.A. Crosby, J. Am. Chem. Soc. 94 (1972) 2606.
[47] B. Durham, J.V. Caspar, J.K. Nagle, T.J. Meyer, J. Am. Chem. Soc. 104 (1982) 4803.
[48] (a) Enraf–Nonius, The Netherland, 1994;
(b) COLLECT Software, Data Collection Software, Nonius BV, Delft, The Netherlands, 1998.
[49] E.J. Gabe, Y. Le Page, J.P. Charland, F.L. Lee, P.S. White, J. Appl. Crystallogr. 22 (1989) 384.
[50] G.M. Sheldrick, SHELXL-97, Program for the Refinement of Crystal Structures, University of Göttingen, Germany, 1997.
[51] A.C. Larson, Crystallographic Computing, Munksgaard, Copenhagen, 1970.